Bulk AlInAs on InP(111) as a novel material system for pure single photon emission

Sebastian Unsleber[1], Michael Deppisch[1], Christian M. Krammel[2], Minh Vo[1], Christopher D. Yerino[3], Paul J. Simmonds[4], Minjoo Larry Lee[3,5], Paul M. Koenraad[2], Christian Schneider[1,*], Sven Höfling[1,6]

[1] *Technische Physik and Wilhelm Conrad Röntgen Research Center for Complex Material Systems, Physikalisches Institut, Universität Würzburg, Am Hubland, D-97074 Würzburg, Germany*
[2] *Department of Applied Physics, Eindhoven University of Technology, Eindhoven 5612 AZ, The Netherlands*
[3] *Department of Electrical Engineering, Yale University, PO Box 208284, New Haven, CT 06520, USA*
[4] *Boise State University, Departments of Physics and Materials Science and Engineering, Boise, ID 83725, USA*
[5] *Department of Electrical and Computer Engineering, University of Illinois at Urbana-Champaign, Urbana, IL 61801, USA*
[6] *SUPA, School of Physics and Astronomy, University of St Andrews, St Andrews, KY16 9SS, United Kingdom*
[*] *christian.schneider@physik.uni-wuerzburg.de*

Abstract:

In this letter, we report on quantum light emission from bulk AlInAs grown on InP(111) substrates. We observe indium rich clusters in the bulk $Al_{0.48}In_{0.52}As$ (AlInAs), resulting in quantum dot-like energetic traps for charge carriers, which are confirmed via cross-sectional scanning tunnelling microscopy (XSTM) measurements and 6-band $\mathbf{k}\cdot\mathbf{p}$ simulations. We observe quantum dot (QD)-like emission signals, which appear as sharp lines in our photoluminescence spectra at near infrared wavelengths around 860 nm, and with linewidths as narrow as 50 μeV. We demonstrate the capability of this new material system to act as an emitter of pure single photons as we extract $g^{(2)}$-values as low as $g^{(2)}_{\mathrm{cw}}(0) = 0.05^{+0.17}_{-0.05}$ for continuous wave (cw) excitation and $g^{(2)}_{\mathrm{pulsed,\ corr.}} = 0.24 \pm 0.02$ for pulsed excitation.

OCIS codes: (270.0270) Quantum optics; (270.5565) Quantum communication; (270.5290) Photon statistics.

References and links

1. C. Bennett and G. Brassard, "Quantum cryptography: Public key distribution and coin tossing," in "International Conference on Computer System and Signal Processing, IEEE, 1984," (1984), pp. 175–179.
2. J. McKeever, A. Boca, A. D. Boozer, R. Miller, J. R. Buck, A. Kuzmich, and H. J. Kimble, "Deterministic generation of single photons from one atom trapped in a cavity," Science **303**, 1992–1994 (2004).
3. F. Diedrich and H. Walther, "Nonclassical radiation of a single stored ion," Phys. Rev. Lett. **58**, 203–206 (1987).
4. R. Brouri, A. Beveratos, J.-P. Poizat, and P. Grangier, "Photon antibunching in the fluorescence of individual color centers in diamond," Opt. Lett. **25**, 1294–1296 (2000).
5. C. Kurtsiefer, S. Mayer, P. Zarda, and H. Weinfurter, "Stable solid-state source of single photons," Phys. Rev. Lett. **85**, 290–293 (2000).
6. T. Basché, W. E. Moerner, M. Orrit, and H. Talon, "Photon antibunching in the fluorescence of a single dye molecule trapped in a solid," Phys. Rev. Lett. **69**, 1516–1519 (1992).
7. M. Ikezawa, Y. Sakuma, and Y. Masumoto, "Single photon emission from individual nitrogen pairs in GaP," Jpn. J. Appl. Phys. **46**, L871 (2007).
8. S. Castelletto, B. Johnson, V. Ivády, N. Stavrias, T. Umeda, A. Gali, and T. Ohshima, "A silicon carbide room-temperature single-photon source," Nat. Mater. **13**, 151–156 (2014).
9. Y.-M. He, G. Clark, J. R. Schaibley, Y. He, C. Ming-Cheng, Y.-J. Wei, X. Ding, Q. Zhang, W. Yao, X. Xu, C.-Y. Lu, and J.-W. Pan, "Single quantum emitters in monolayer semiconductors," Nat. Nanotechnol. **10**, 497–502 (2015).

10. P. Tonndorf, R. Schmidt, R. Schneider, J. Kern, M. Buscema, G. A. Steele, A. Castellanos-Gomez, H. S. J. van der Zant, S. M. de Vasconcellos, and R. Bratschitsch, "Single-photon emission from localized excitons in an atomically thin semiconductor," Optica **2**, 347–352 (2015).
11. A. Srivastava, M. Sidler, A. V. Allain, D. S. Lembke, A. Kis, and A. Imamoğlu, "Optically active quantum dots in monolayer WSe_2," Nat. Nanotechnol. **10**, 491–496 (2015).
12. C. Chakraborty, L. Kinnischtzke, K. M. Goodfellow, R. Beams, and A. N. Vamivakas, "Voltage-controlled quantum light from an atomically thin semiconductor," Nat. Nanotechnol. **10**, 507–511 (2015).
13. M. Koperski, K. Nogajewski, A. Arora, V. Cherkez, P. Mallet, J.-Y. Veuillen, J. Marcus, P. Kossacki, and M. Potemski, "Single photon emitters in exfoliated WSe_2 structures," Nat. Nanotechnol. **10**, 503–506 (2015).
14. P. Michler, A. Kiraz, C. Becher, W. V. Schoenfeld, P. M. Petroff, L. Zhang, E. Hu, and A. Imamoglu, "A quantum dot single-photon turnstile device," Science **290**, 2282–2285 (2000).
15. C. Santori, M. Pelton, G. Solomon, Y. Dale, and Y. Yamamoto, "Triggered single photons from a quantum dot," Phys. Rev. Lett. **86**, 1502–1505 (2001).
16. J. M. Gérard, B. Sermage, B. Gayral, B. Legrand, E. Costard, and V. Thierry-Mieg, "Enhanced spontaneous emission by quantum boxes in a monolithic optical microcavity," Phys. Rev. Lett. **81**, 1110–1113 (1998).
17. S. Reitzenstein and A. Forchel, "Quantum dot micropillars," J. Phys. D: Appl. Phys. **43**, 033001 (25pp) (2010).
18. S. Unsleber, Y.-M. He, S. Gerhardt, S. Maier, C.-Y. Lu, J.-W. Pan, N. Gregersen, M. Kamp, C. Schneider, and S. Höfling, "Highly indistinguishable on-demand resonance fluorescence photons from a deterministic quantum dot micropillar device with 74% extraction efficiency," Opt. Express **24**, 8539–8546 (2016).
19. J. Claudon, J. Bleuse, N. S. Malik, M. Bazin, P. Jaffrennou, N. Gregersen, C. Sauvan, P. Lalanne, and J.-M. Gerard, "A highly efficient single-photon source based on a quantum dot in a photonic nanowire," Nat. Photonics **4**, 174–177 (2010).
20. M. E. Reimer, G. Bulgarini, N. Akopian, M. Hocevar, M. B. Bavinck, M. A. Verheijen, E. P. Bakkers, L. P. Kouwenhoven, and V. Zwiller, "Bright single-photon sources in bottom-up tailored nanowires," Nat. Commun. **3**, 737– (2012).
21. M. Arcari, I. Söllner, A. Javadi, S. Lindskov Hansen, S. Mahmoodian, J. Liu, H. Thyrrestrup, E. H. Lee, J. D. Song, S. Stobbe, and P. Lodahl, "Near-unity coupling efficiency of a quantum emitter to a photonic crystal waveguide," Phys. Rev. Lett. **113**, 093603 (2014).
22. E. Waks, K. Inoue, C. Santori, D. Fattal, J. Vuckovic, G. S. Solomon, and Y. Yamamoto, "Quantum cryptography with a photon turnstile," Nature (2002).
23. T. Heindel, C. A. Kessler, M. Rau, C. Schneider, M. Fürst, F. Hargart, W.-M. Schulz, M. Eichfelder, R. Roßbach, S. Nauerth, M. Lermer, H. Weier, M. Jetter, M. Kamp, S. Reitzenstein, S. Höfling, P. Michler, H. Weinfurter, and A. Forchel, "Quantum key distribution using quantum dot single-photon emitting diodes in the red and near infrared spectral range," New J. Phys. **14**, 083001 (2012).
24. M. Rau, T. Heindel, S. Unsleber, T. Braun, J. Fischer, S. Frick, S. Nauerth, C. Schneider, G. Vest, S. Reitzenstein, M. Kamp, A. Forchel, S. Höfling, and H. Weinfurter, "Free space quantum key distribution over 500 meters using electrically driven quantum dot single-photon sources– a proof of principle experiment," New J. Phys. **16**, 043003 (2014).
25. S. Birner, T. Zibold, T. Andlauer, T. Kubis, M. Sabathil, A. Trellakis, and P. Vogl, "Nextnano: general purpose 3-D simulations," Electron Devices, IEEE Transactions on **54**, 2137–2142 (2007).
26. C. D. Yerino, P. J. Simmonds, B. Liang, D. Jung, C. Schneider, S. Unsleber, M. Vo, D. L. Huffaker, S. Höfling, M. Kamp, and M. L. Lee, "Strain-driven growth of GaAs (111) quantum dots with low fine structure splitting," Appl. Phys. Lett. **105**, 251901 (2014).
27. Q. Wu, G. D. Feke, R. D. Grober, and L. P. Ghislain, "Realization of numerical aperture 2.0 using a gallium phosphide solid immersion lens," Appl. Phys. Lett. **75**, 4064–4066 (1999).
28. D. Bimberg, M. Sondergeld, and E. Grobe, "Thermal dissociation of excitons bounds to neutral acceptors in high-purity GaAs," Phys. Rev. B **4**, 3451 (1971).
29. P. Offermans, P. M. Koenraad, J. H. Wolter, K. Pierz, M. Roy, and P. A. Maksym, "Atomic-scale structure and photoluminescence of InAs quantum dots in GaAs and AlAs," Phys. Rev. B **72**, 165332 (2005).
30. A. Lenz, R. Timm, H. Eisele, C. Hennig, S. Becker, R. Sellin, U. Pohl, D. Bimberg, and M. Dähne, "Reversed truncated cone composition distribution of $In_{0.8}Ga_{0.2}As$ quantum dots overgrown by an $In_{0.1}Ga_{0.9}As$ layer in a GaAs matrix," Appl. Phys. Lett. **81**, 5150–5152 (2002).
31. A. Giddings, J. Keizer, M. Hara, G. Hamhuis, H. Yuasa, H. Fukuzawa, and P. Koenraad, "Composition profiling of InAs quantum dots and wetting layers by atom probe tomography and cross-sectional scanning tunneling microscopy," Phys. Rev. B **83**, 205308 (2011).
32. A. Wijnheijmer, J. Garleff, K. Teichmann, M. Wenderoth, S. Loth, and P. Koenraad, "Single Si dopants in GaAs studied by scanning tunneling microscopy and spectroscopy," Phys. Rev. B **84**, 125310 (2011).
33. S. Ates, S. M. Ulrich, S. Reitzenstein, A. Löffler, A. Forchel, and P. Michler, "Post-selected indistinguishable photons from the resonance fluorescence of a single quantum dot in a microcavity," Phys. Rev. Lett. **103**, 167402 (2009).
34. D. Richter, R. Hafenbrak, K. D. Jöns, W.-M. Schulz, M. Eichfelder, M. Heldmaier, R. Roßbach, M. Jetter, and P. Michler, "Low density movpe grown InGaAs QDs exhibiting ultra-narrow single exciton linewidths," Nanotechnology **21**, 125606 (2010).

35. M. Bayer and A. Forchel, "Temperature dependence of the exciton homogeneous linewidth in $In_{0.60}Ga_{0.40}As/GaAs$ self-assembled quantum dots," Phys. Rev. B **65**, 041308 (2002).
36. A. V. Uskov, I. Magnusdottir, B. Tromborg, J. Mo/rk, and R. Lang, "Line broadening caused by coulomb carrier-carrier correlations and dynamics of carrier capture and emission in quantum dots," Appl. Phys. Lett. **79**, 1679–1681 (2001).
37. S. Unsleber, S. Maier, D. P. S. McCutcheon, Y.-M. He, M. Dambach, M. Gschrey, N. Gregersen, J. Mørk, S. Reitzenstein, S. Höfling, C. Schneider, and M. Kamp, "Observation of resonance fluorescence and the mollow triplet from a coherently driven site-controlled quantum dot," Optica **2**, 1072–1077 (2015).
38. P. Gold, A. Thoma, S. Maier, S. Reitzenstein, C. Schneider, S. Höfling, and M. Kamp, "Two-photon interference from remote quantum dots with inhomogeneously broadened linewidths," Phys. Rev. B **89**, 035313 (2014).
39. A. Schliwa, M. Winkelnkemper, A. Lochmann, E. Stock, and D. Bimberg, "In(Ga)As/GaAs quantum dots grown on a (111) surface as ideal sources of entangled photon pairs," Phys. Rev. B **80**, 161307 (2009).
40. R. Singh and G. Bester, "Nanowire quantum dots as an ideal source of entangled photon pairs," Phys. Rev. Lett. **103**, 063601 (2009).
41. E. Stock, T. Warming, I. Ostapenko, S. Rodt, A. Schliwa, J. A. Töfflinger, A. Lochmann, A. I. Toropov, S. A. Moshchenko, D. V. Dmitriev, V. A. Haisler, and D. Bimberg, "Single-photon emission from InGaAs quantum dots grown on (111) GaAs," Appl. Phys. Lett. **96**, 093112 (2010).
42. J. Treu, C. Schneider, A. Huggenberger, T. Braun, S. Reitzenstein, S. Höfling, and M. Kamp, "Substrate orientation dependent fine structure splitting of symmetric In(Ga)As/GaAs quantum dots," Appl. Phys. Lett. **101**, 022102 (2012).
43. S. Seidl, B. Gerardot, P. Dalgarno, K. Kowalik, A. Holleitner, P. Petroff, K. Karrai, and R. Warburton, "Statistics of quantum dot exciton fine structure splittings and their polarization orientations," Physica E **40**, 2153–2155 (2008).
44. R. Seguin, A. Schliwa, S. Rodt, K. Pötschke, U. W. Pohl, and D. Bimberg, "Size-dependent fine-structure splitting in self-organized $InAs/GaAs$ quantum dots," Phys. Rev. Lett. **95**, 257402 (2005).
45. K. Kowalik, O. Krebs, A. Lemaitre, S. Laurent, P. Senellart, P. Voisin, and J. Gaj, "Influence of an in-plane electric field on exciton fine structure in InAs-GaAs self-assembled quantum dots," Appl. Phys. Lett. **86**, 1907 (2005).
46. P. Michler, A. Imamoglu, A. Kiraz, C. Becher, M. Mason, P. Carson, G. Strouse, S. Buratto, W. Schoenfeld, and P. Petroff, "Nonclassical radiation from a single quantum dot," Phys. Status Solidi B **229**, 399–405 (2002).

1. Introduction

One of the key components in quantum cryptography schemes like the BB84 protocol [1] is an emitter of single photons. In recent decades, enormous effort has been spent identifying possible sources of single quanta of light.

Researchers have explored a variety of material systems including cold atoms [2], trapped ions [3], colour centres in diamond [4, 5], single molecules [6], nitrogen pairs in GaP [7], silicon carbide [8], layered materials [9–13] and semiconductor QDs [14, 15]. Comparing all these sources, a semiconductor based device offers several advantages. First, the quantum emitter can be implemented into scalable cavity structures like QDs in micropillar cavities [16–18] or photonic waveguides [19–21]. Second, successful proof-of-principle quantum key distribution experiments using QD-based sources have already been demonstrated [22–24]. While the epitaxial growth of low density InGaAs or InP QDs is well established nowadays, it still relies on extremely close control of growth parameters. Within a deviation of less than one nanometer of deposited material, an InGaAs QD layer can either fully relax, or the critical thickness for QD formation may not even be reached. This naturally reduces the yield of excellent QD samples, in particular if no in-situ growth control mechanisms (such as RHEED) are available. In this work, we report on a novel material system for single photon emission with a remarkably straightforward fabrication technique that relies simply on growing a single volume of bulk material. We observe discrete, QD-like emission lines from 200 nm thick AlInAs-layers grown on InP(111) substrates. We identify excitons trapped in indium-rich nanoclusters as the origin of these emission features via XSTM measurements and *nextnano++* simulations [25]. Furthermore, we present a detailed investigation of these novel emission features, and show spectrally sharp emission lines with a median linewidth of 137 μeV, and moderate fine structure splitting (FSS) with a median value of 28 μeV. Probing the photon statistics of the emission features, we can confirm pure single photon emission with $g^{(2)}$-values as low as $g^{(2)}_{\mathrm{cw}}(0) = 0.05^{+0.17}_{-0.05}$ for cw and $g^{(2)}_{\mathrm{pulsed,\ corr.}} = 0.24 \pm 0.02$ for pulsed excitation.

2. Sample fabrication and experimental setup

Our samples are grown on nominally exact InP(111) substrates via molecular beam epitaxy. In order to smooth the substrate surface, a 50 nm thick $In_{0.53}Ga_{0.47}As$ (InGaAs) layer is grown on the InP [26]. Afterwards a 200 nm thick AlInAs layer is deposited. The initial samples where we first observed the atom-like emission features, also contained a layer of (111)-oriented GaAs QDs together with a 100 nm thick capping layer to passivate the QDs. We have demonstrated that these (111)-oriented QDs emit photons in the spectral range above 950 nm, i.e. redshifted by 100 nm compared with the localization centers which we discuss in this work [26]. To increase the outcoupling efficiency of light during spectroscopic measurements, a solid immersion lens was glued on top of the sample with mounting wax. This leads to a higher numerical aperture and therefore increases the amount of emitted photons which are guided into the microscope objective [27]. As reference for the micro-photoluminescence (μPL) investigations, we used a sample with 1 μm AlInAs on InP(001) to investigate the role of substrate orientation in the generation of these spectrally sharp emission features.

For the μPL measurements the sample was mounted on the cold finger of a *l*He-flow cryostat and pumped either with a frequency doubled, cw Nd:YAG-laser ($\lambda = 532$ nm) or a frequency doubled, pulsed Ti:Sapphire-laser ($\lambda = 475$ nm, repetition rate 82 MHz). The collected photons were analysed with a monochromator with a 1500 $\frac{\text{lines}}{\text{mm}}$ grating ($\Delta E_{\text{Res}} \approx 30$ μeV) for the high resolution images or a 300 $\frac{\text{lines}}{\text{mm}}$ grating for overview spectras. At the output port of the monochromator, a fiber coupled Hanbury Brown and Twiss setup (HBT) with a timing resolution of approximately 570 ps is implemented to measure the second order field correlation of the emission.

All the XSTM work was performed in a commercial Omicron low temperature STM at 77 K. The XSTM measurement was carried out in constant current mode on (110) surfaces generated by in-situ cleavage at pressures below $4\text{x}10^{-11}$ mbar. Electrochemically etched polycrystalline tungsten tips cleaned in-situ by annealing and Ar-sputtering were used. During the XSTM measurements the carrier density in the sample was additionally increased by photo excitation with an external light source.

3. Experimental results

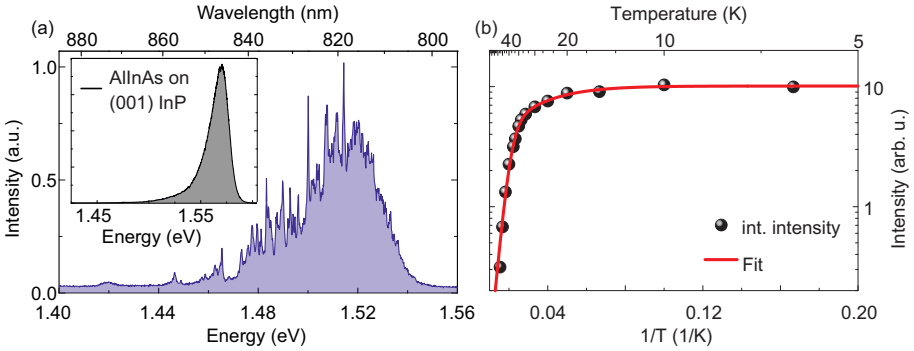

Fig. 1. (a) μPL spectrum of a sample with a 200 nm thick AlInAs layer which is grown on InP(111). The spectra breaks up into an ensemble of discrete emitter lines, similar to a QD-ensemble. The inset shows a reference sample with AlInAs grown on InP(001) demonstrating the absence of any discrete emission features. (b) Temperature dependent emission intensity of a selected, spectrally isolated AlInAs-cluster line. The fit (see equ. 1) reveals two decay channels with activation energies of $E_1 = 34 \pm 4$ meV and $E_2 = 5 \pm 1$ meV.

Figure 1(a) shows a μPL spectrum from an AlInAs/InP(111) sample for a temperature of $T = 10$ K. The high density of sharp spectral features in the spectrum near the AlInAs bandgap suggests the emission from QD-like nanostructures. As we will show, these nanostructures are In-rich clusters that form spontaneously during the growth of AlInAs(111). A higher indium amount leads to a local decrease of the bandgap and therefore to a three dimensional confinement for charge carriers. The inset of Fig. 1(a) shows the emission from the AlInAs/InP(001) reference sample for a temperature of $T = 10$ K. The absence of the spectrally sharp emission lines shows that these lines are unique to the (111) AlInAs sample. We thus conclude, that the formation of this nanoclusters is driven by strain in the AlInAs layer which is only present for the (111) growth direction and the formation of indium rich nanoclusters is a mechanism to relax this strain. Furthermore, the AlInAs growth is dominated by 2D island nucleation, which results in a high density of step-edges [26]. These edges present many sites for incoming adsorbed atoms and therefore may also lead to a formation of indium and aluminium rich clusters due to the different mobility of the adsorbed atoms. As a first characterisation step, we measured the integrated intensity of a single, spectrally isolated AlInAs-cluster while varying the sample temperature. Figure 1(b) shows the integrated intensity versus the inverse temperature. We observe a decrease of the intensity with increasing temperature due to the thermal activation of the charge carriers. In order to extract the activation energy for the loss channels, we assume two possible channels with activation energies E_1 and E_2. From solving a simple rate equation model, one obtains [28]

$$I(T) = I_0 * \left(1 + C_1 \cdot \mathrm{e}^{-\frac{E_1}{k_B T}} + C_2 \cdot \mathrm{e}^{-\frac{E_2}{k_B T}}\right)^{-1}, \tag{1}$$

where I_0 is the intensity of the signal at 0 K, C_1 and C_2 describe the strength of both decay channels, k_B is the Boltzmann constant and T is the temperature. The fit of Fig. 1(b) is in very good agreement with the measured data and we can extract activation energies of $E_1 = 34 \pm 4$ meV and $E_2 = 5 \pm 1$ meV, which we attribute to the thermal activation of the bound electron respectively hole. For all lines we investigated, the two decay channels showed activation energies of ≈ 5 meV and ≈ 30 meV.

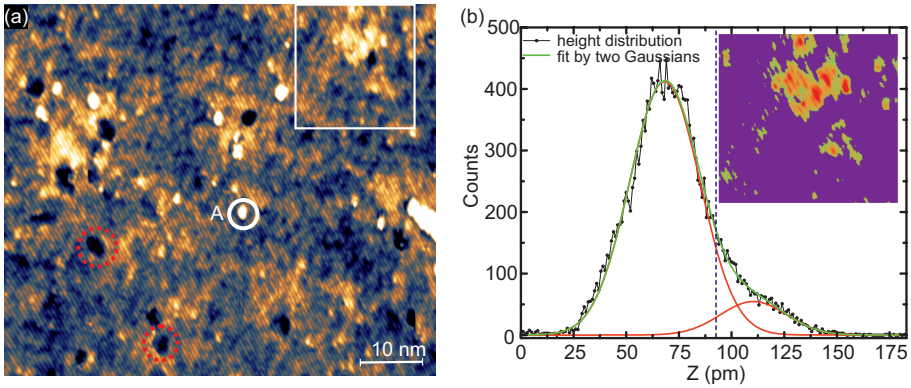

Fig. 2. (a) High resolution filled-state XSTM image of AlInAs grown on (111)InP, which is taken at a voltage between sample and tip of $U_S = -2.6$ V and a tunnelling current of $I_T = 30$ pA. In-rich regions appear bright and Al-rich areas dark. An adsorbent (A) on the surface is highlighted as an example. (b) Height distribution of the region marked in (a) with a white rectangle. The green line is a fit of the height distribution by two Gaussians (red). In the inset all heights below the half-width height of the smaller Gaussian, which is indicated by a dashed blue line, are clipped.

In order to test our hypothesis, that these sharp lines are emitted by bound excitons in indium

rich clusters, we performed XSTM measurements. In Fig. 2(a) a typical filled-state XSTM image of AlInAs grown on (111) InP is shown. The image is taken at high negative sample voltages. When imaging at these tunnelling conditions the electronic contrast is strongly suppressed and the real deformation of the surface is dominant [29, 30]. InAs has a larger lattice constant than AlAs and the compressive strain in the In rich regions of the AlInAs layer leads to an outward relaxation of the surface in these zones. In-rich areas appear bright in Fig. 2(a) and deeper lying Al-rich ones dark. This gives clear evidence for the spontaneous formation of large scale compositional fluctuations in the form of In-rich clusters within the AlInAs layer. To establish a connection between these compositional fluctuations and the observed optical properties of the sample, detailed knowledge about their dimensions and composition is required. A structural analysis reveals strong variations in the dimensions of the In-rich clusters. In the statistics, In-rich regions that are too small are not considered, as these are most likely related to an off-center cleavage during XSTM sample preparation. The larger In-rich clusters are found to be about 16 nm in diameter. Conclusions on the magnitude of the In fluctuations in the larger clusters can be drawn from the relaxation of the cleaved surface. This method was used in earlier works for compositional studies of QDs and wetting layers by XSTM [29, 30]. To get a measure for the relaxation in the In-rich regions, the height distribution in a small region around the In-rich clusters is fitted by two Gaussians. An example is shown in Fig. 2(b) for the area marked with a white rectangle. In the inset all heights below the half maximum height of the smaller Gaussian are clipped (dashed blue line in Fig. 2(b)). This illustrates that the larger Gaussian is related to the AlInAs matrix and the smaller Gaussian to the In-rich clusters. In this way an outward relaxation at the bigger cluster of about (54 ± 16) pm is found, which is given by the difference of the Gaussian centers. COMSOL simulations for the surface relaxation of the In-rich regions show that their composition is close to $Al_{0.40}In_{0.60}As$ [29, 31]. For the simulations, we assumed the surrounding material to be the nominal $Al_{0.48}In_{0.52}As$ composition. The nominal composition was calibrated via x-ray diffraction after growing the samples. Apart from the large scale compositional fluctuations in the immediate vicinity of the In-rich cluster smaller structures with a dark contrast are found. We exemplary marked two of these dark areas with a red ring in Fig. 2(a). The atomic rows continue throughout the dark structures and their surrounding matrix. This excludes spots where material was ripped out during cleavage. At a monoatomic step on the (110) surface the atomic corrugation would be shifted by half a lattice constant. In addition, the sharp jagged edges of the dark objects point against charging effects as seen at donors or acceptors [32]. Accordingly, these highly localized dark objects must be attributed to In-poor (i.e., Al-rich) spots in the AlInAs layer. It appears that In- and Al- rich areas in the AlInAs facilitate each other as a mechanism to relax local strain in the AlInAs layer.

In order to support the results from the XSTM measurements, we simulated indium rich clusters in an AlInAs layer with the commercial tool *nextnano++*, which uses a 6-band $\mathbf{k}\cdot\mathbf{p}$ approximation to simulate the band structure and then calculates the energetic ground state. We simulated spherical clusters of three different diameters, namely 12 nm, 16 nm and 20 nm. The indium content within the cluster was varied from 56 % to 62 %. For the simulations we also assumed constant compositions in every part of the simulated structure. Figure 3(a) shows the simulated band structure of a 16 nm cluster with an In content of 60 %. The energy difference between the electron and hole ground state is found to be $\Delta E = 1.45$ eV and fits therefore very well with the sharp emission lines in the spectrum of Fig. 1(a). Our analysis of Fig. 1(b) showed that both electron and hole states are very well confined inside the cluster, which is confirmed by the simulated density of the wave function in Fig.3(a). The depth of the confinement is approximately 60 meV for the electron and 20 meV for the hole state, which is slightly larger, than the two activation energies found by temperature dependent μPL measurements in Fig. 1(b). The reason for this slight deviation could originate in several limitations of our simulation. First, our simulated structure is an approximation of the results

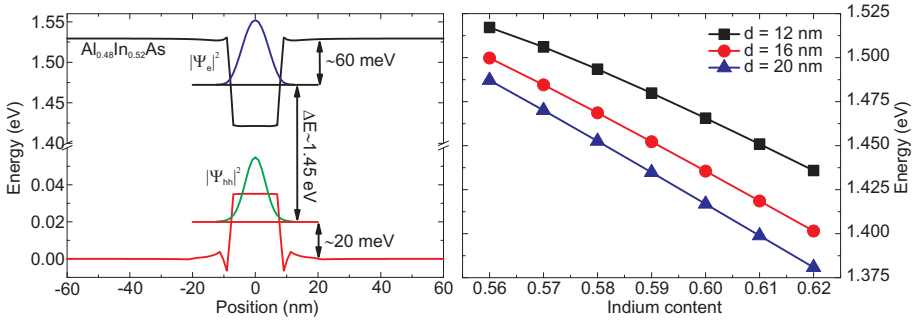

Fig. 3. (a) Simulated band structure of a 16 nm diameter cluster with an In content of 60 %. The result is a confined state for both electron and hole, with confinement energies of approximately 60 meV and 20 meV. The resulting energy gap between the two confined states is simulated to be 1.45 eV, which fits very well to the μPL-data and the In-rich clusters seen in XSTM. (b) Energy difference between the two confined states as a function of the In-content for three different cluster sizes.

found by XSTM-measurements. We simulated a discrete step in the indium concentration which is an approximation of the more gentle transition to indium-rich regions found by XSTM measurements. Second, our simulations neglect carrier-carrier interactions which also influences the transition energies as well as the activation energies. The resulting transition energy from our simulations of the ground state for varying diameter and In-content is plotted in Fig. 3(b). Our simulations show an energy range of approximately 1.38 eV to 1.52 eV for the transition energy, which is in very good agreement with the observed energy range of the sharp emission lines in Fig. 1(a) ($\approx 1.45-1.53$ eV). The simulated depth of the confinement ranges from $10-100$ meV for the electron and $5-35$ meV for the hole state, which covers the values found in Fig. 1(b). These simulations confirm that the QD-like emission features from our sample originate from In-rich clusters which spontaneously form inside the bulk AlInAs layer.

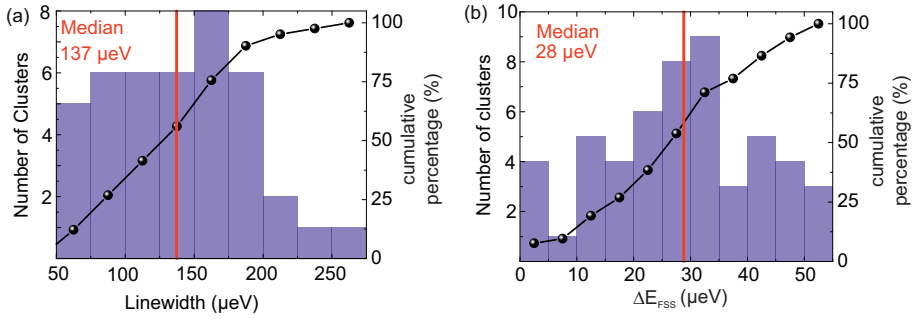

Fig. 4. (a) Statistic of the linewidth distribution. We extract a median linewidth of 137 μeV for the AlInAs-cluster emission lines. (b) Summary of the excitonic FSS. A median FSS of $FSS_{Median} = 28.5$ μeV is extracted from the analysis of 52 emission lines.

Next, we analysed the linewidth of the clusters for non resonant excitation with a green laser. The statistical overview is shown in Fig. 4(a). We find a median full width at half maximum (FWHM) linewidth of $FWHM_{\text{median}} = 137$ μeV where the narrowest line has a linewidth of $FWHM_{\text{Min}} = (54 \pm 4)$ μeV. These linewidths are higher than typically reported values of < 10 μeV for self organized InGaAs QDs [33–35]. The Gaussian profile which we observe for most of the emission lines suggests that the emission is broadened by spectral diffusion [36]. We

believe these values can be optimized using quasi- or strictly resonant excitation as reported for InGaAs-QDs [33, 37, 38].

The (111) growth direction leads to QDs with a a higher symmetry of the excitonic wave functions and therefore to a vanishing FSS between the exciton emission energies, due to the threefold symmetry and internal piezoelectric field along the growth direction [39–42]. In order to verify whether the AlInAs-clusters offer similar symmetry features to other (111)-QDs, we measured the FSS of the exciton. For these measurements we carried out high resolution μPL measurements with an additional $\lambda/2$ wave plate and a linear polarizer (set to the high reflectivity axis of the grating) in the beampath. Fitting each spectrum with a Gaussian profile one obtains the polarizer-dependent central energy of the emission line. If the cluster exhibits finite FSS, we observe a sinusoidal response (see e.g. Fig. 4(b) in 26). From the peak to peak distance we can extract the FSS of the exciton. We carefully analysed many of these measurements resulting in 52 lines included in our statistics and plotted in Fig. 4(b). Measurements are only included where we could observe a clear sinusoidal trend. We find a median splitting of the exciton states of $\Delta E_{FSS,\mathrm{median}} = 28.5$ μeV. This is slightly larger than for GaAs(111) QDs grown on InP(111)-substrate (median FSS 7.6 μeV, see [26]) and In(Ga)As-QDs on GaAs(111) substrate (median FSS 5.6 μeV, see [42]), but comparable to standard In(Ga)As-QDs grown on GaAs(001) substrates (typically a few 10 μeV up over 100 μeV) [35, 42–45]. We thus conclude, that the carrier confinement symmetry is $C_{2\theta}$ or lower and the AlInAs nanoclusters do not preserve the threefold symmetry which is predicted for (111)-grown QDs [39]

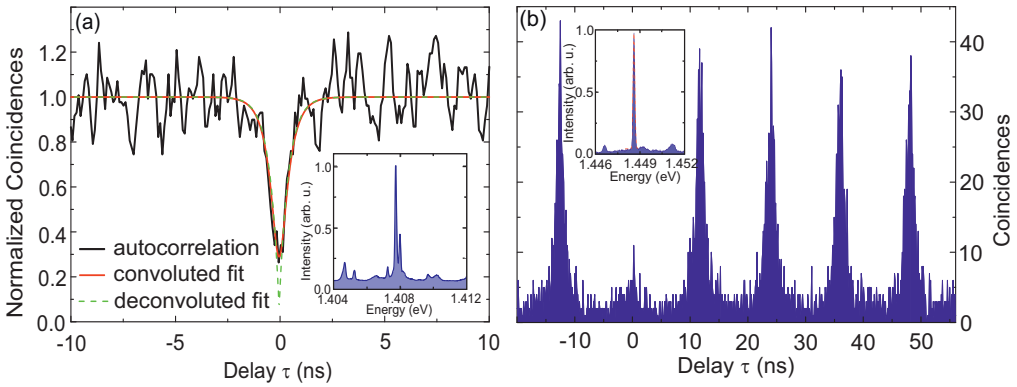

Fig. 5. (a) CW pumped autocorrelation of the emission line shown in the inset. The dip around $\tau \approx 0$ ns reaches down well below 0.5 which demonstrates the single photon emission properties. Fitting the normalized coincidences with equ. 3 we obtain a deconvoluted $g^{(2)}(0)$-value of $g^{(2)}_{\mathrm{cw}} = 0.05^{+0.17}_{-0.05}$. (b) Pulsed autocorrelation histogram of the AlInAs-cluster emission line shown in the inset. Dividing the area of the central peak through the average area of the surrounding peaks and correction for spectral background emission, we obtain $g^{(2)}_{\mathrm{pulsed,\ corr.}} = 0.24 \pm 0.02$.

In terms of the potential for applications in quantum information technology, it is essential that the AlInAs-clusters act as emitters of single photons. Figure 5(a) shows the cw-pumped autocorrelation histogram from a single AlInAs-cluster whose emission spectrum is shown in the inset. The emission is spectrally filtered by a monochromator and then coupled into a fiber-based HBT-setup to measure the second order autocorrelation. Around $\tau \approx 0$ ns a clear dip is observable which reaches down well below 0.5 and therefore proves single photon emission. In order to account for the finite timing resolution of our setup, we fit the measured data with a two sided

exponential decay convolved with a Gaussian distribution f_{Det}:

$$g^{(2)}_{source}(\tau) = 1-((1-g^{(2)}(0))*e^{-|\frac{\tau}{\tau_C}|}) \quad (2)$$

$$g^{(2)}_{measured}(\tau) = (g^{(2)}_{source}*f_{Det})(\tau) \quad (3)$$

The convolved (red) and deconvolved (green) fit functions are also plotted in Fig. 5(a). We extract a deconvoluted $g^{(2)}(0)$-value of $g^{(2)}_{cw} = 0.05^{+0.17}_{-0.05}$. We attribute the slight imperfection to an overlap with a second emission line on the high energy side of the measured line.
Triggered single photon emission is confirmed by measuring the second order autocorrelation function for a pulsed excitation scheme. The Nd:YAG-laser was substituted with a frequency-doubled Ti:sapphire laser emitting around $\lambda = 475$ nm with a repetition rate of $f_{Rep} = 82$ MHz. Figure 5(b) shows the coincidence histogram for pulsed excitation of the cluster emission shown in the inset. From the measured histogram, we extract the $g^{(2)}(0)$-value by summarizing the coincidences within each 12.2 ns wide time window and dividing the area of the central peak at $\tau = 0$ ns by the average area of the surrounding peaks. From this evaluation we obtain $g^{(2)}_{\text{pulsed}}(0) = 0.35 \pm 0.02$, which confirms triggered single photon emission. We attribute the deviation from a perfect single photon source to spectral background emission and refilling of the ground state due to the non-resonant excitation scheme. The correlation function $g^{(2)}_b(\tau)$ in the presence of background emission can be described via

$$g^{(2)}_b(\tau) = 1+\rho^2(g^{(2)}(\tau)-1), \quad (4)$$

where $\rho = \frac{S}{S+B}$ represents the signal-to-noise ratio (S: signal counts; B: background counts) [46]. From the spectrum, shown in the inset of Fig. 5(b), we obtain a signal-to-noise ratio of $\rho = 0.92$. This results in a background corrected $g^{(2)}(0)$-value of $g^{(2)}_{\text{pulsed, corr.}} = 0.24 \pm 0.02$. Remaining coincidences are most likely due to a refilling effect because of the non resonant excitation scheme.

4. Conclusion

In conclusion, we have presented a novel material system for the generation of triggered single photons based on the natural formation of indium rich clusters in bulk AlInAs when grown on InP(111) substrate. We confirmed that these clusters are the source of the non-classical light emission using both XSTM and simulations of the electronic ground state. The emission properties feature a median FSS as low as 28.5 μeV and narrow linewidths down to $FWHM_{Min} = (54 \pm 4)$ μeV for above bandgap excitation. Furthermore we have shown single photon emission under cw excitation with a $g^{(2)}(0)$-value as low as $g^{(2)}(0) = 0.05^{+0.17}_{-0.05}$, and triggered single photon emission as pure as $g^{(2)}(0) = 0.24 \pm 0.02$. For future applications, we anticipate that one can control the emission wavelength of these nanoclusters via varying the growth parameters or applying annealing steps.

Funding

State of Bavaria and the German Ministry of Education and Research (BMBF): Project Q.com-H; Chist-era: Program SSQN